J. Earth Syst. Sci. (2019) 128:234
https://doi.org/10.1007/s12040-019-1254-y

EPMA monazite geochronology of the granulites from Daltonganj, eastern India and its correlation with the Rodinia supercontinent

Ravi Ranjan Kumar* and S B Dwivedi

Department of Civil Engineering, Indian Institute of Technology (BHU), Varanasi 221 005, India.
**Corresponding author. e-mail: ravirk.rs.civ16@itbhu.ac.in*

MS received 20 June 2018; revised 26 May 2019; accepted 18 June 2019; published online 5 September 2019

We report the monazite dates of the granulites from Daltonganj (Palamau), Chhotanagpur granite–gneiss complex (CGGC) which covers the significant part of the granulite blocks in central India by using an electron micro probe analyser dating. The monazite grain varies between 70 and 80 μm and shows the distribution of U, Th and Pb in all monazite grains of both samples. Two different dates were obtained from different monazite grains; the first age suggests that the granulite from CGGC preserves the first remnant of the protolith of the Mesoproterozoic era at ∼1424 Ma and second one at ∼972 Ma which provides evidence of metamorphism of the protolith. The CGGC rocks preserve four regional metamorphic events, namely M_1, M_2, M_3 and M_4. But in this work, two different ages from the Daltonganj granulites were obtained which are similar to the M_2 (<1500 Ma, i.e., the age of protolith of the granulitic gneiss) and M_3 (1200–930 Ma) metamorphic events as reported in the CGGC. The M_3 metamorphism attained its average P–T condition at ∼7.35 kbar/792°C, and it represents the prograde metamorphic event. The M_3 metamorphic event supported the Grenville-orogeny, and it was responsible for the metamorphism of the magmatic protolith of granulitic gneiss from the CGGC at the time of amalgamation of the Rodinia supercontinent. The Rodinia assembly had occurred through the global Grenville-orogenic events between 1100 and 900 Ma, with continental blocks which exist at that time.

Keywords. Monazite dating; CGGC; P–T condition; Rodinia assembly.

1. Introduction

Electron micro probe analyser (EPMA) monazite dating has been extensively used for metamorphic and igneous rocks from the last few decades (Suzuki and Adachi 1991, 1994; Montel *et al.* 1994, 1996; Cocherie *et al.* 1997). An electron microprobe of thorium (Th)–uranium (U)–lead (Pb) monazite dating principal was applied to obtain the age of granulite rocks from Daltonganj. Monazite mineral is a phosphate of light weight rare-earth element [(LREE) PO_4], with abundant U, Th and little Pb (Parrish 1990). The rapid accumulation of radiogenic lead (*Pb), to a required level, is possible, which can be analysed with an electron probe (Montel *et al.* 1996). Monazite dating with the help of an electron microprobe has been performed by several researchers based on the abundance of Th, U and Pb (Suzuki and Adachi 1991, 1994; Montel *et al.* 1996; Braun

Supplementary materials pertaining to this article are available on the Journal of Earth Science Website (http://www.ias.ac.in/Journals/Journal_of_Earth_System_Science).

et al. 1998; Williams *et al.* 1999). The EPMA-monazite dating technique is a reliable technique to identify the recorded history of polymetamorphic events (Rosa-Costa *et al.* 2008; Karmakar *et al.* 2011; Prabhakar 2013; Bhowmik *et al.* 2014). Petrogenetic considerations and the textural relations of mineral phases in the granulite of the Chhotanagpur granite–gneiss complex (CGGC) suggest that M_1 (1700–1600 Ma) and M_4 (1000–900 Ma) are the prograde metamorphic events, which are separated by M_2 and M_3 (1100–1400 Ma) retrograde metamorphic events (Maji *et al.* 2008), and they are of younger age (830–600 Ma), the cause of which remains unexplored. Furthermore, Sanyal and Sengupta (2012) documented the four metamorphic stages (M_1–M_4), where the M_1 metamorphic stage occurred around 1870 Ma and successively followed by the M_2 metamorphic phase between 1660 and 1270 Ma, the M_3 phase was recorded between 1200 and 930 Ma, followed by an M_4 event at 870–780 Ma. The detail of the four metamorphic stages along with their age and technique of dating by various authors in CGGC is given in table 1.

Chatterjee *et al.* (2010) correlated the Precambrian eastern Indian terrain with the Sausar mobile belt in central India and the Shillong–Meghalaya granulite belt from the north-eastern part of India which can be used as an essential tool for the India–Australia–Antarctica correlation. The breakdown of the Columbia supercontinent was initiated during the Mesoproterozoic era which leads to the reconstruction of the Rodinia supercontinent between 1200 and 900 Ma (Dalziel 1991; Hoffman 1991; Moores 1991; Li *et al.* 2008; Bhowmik *et al.* 2010). Greater India is shown to have been in contact with the Antarctica–Australia Peri–Rodinian margin (Li *et al.* 2008) supported by the petrological and geochronological setting of the Eastern Ghats mobile belt (EGMB) of India and the Rayner province of Antarctica (Dalziel 1991; Yoshida *et al.* 1992; Shaw *et al.* 1997; Mezger and Cosca 1999; Dasgupta and Sengupta 2003). 1000–900 Ma age was preserved in older high-pressure metamorphic rocks of CGGC which is assumed to be the extension of central Indian tectonic zone (CITZ), and act as a suture zone when the SIB, NIB and MC were joined together during the Stenian–Tonian orogenesis (Bhowmik *et al.* 2010). Polymetamorphic events were preserved in the SIB, CITZ and CGGC with similarity with respect to petrological and geochronological properties (Chatterjee *et al.* 2008; Maji *et al.* 2008; Sanyal and Sengupta 2012). This study deals with the electron microprobe monazite dating of the garnet–hypersthene–gedrite–cordierite gneiss and the garnet–gedrite–cordierite–biotite gneiss from Daltonganj (Palamau) in the CGGC. We have documented the evidence of the tectono-metamorphic event from the north-western part of CGGC with the help of petrological, geothermobarometry and EPMA-monazite dating techniques. We have also striven to unravel the geodynamic implications of metamorphism in the granulite facies rocks of CGGC and their correlation to global-scale Grenvillian orogenesis suturing in the peninsular part of India with the Rodinia assembly.

2. Geological background

The area under investigation (latitude 23°54′50″–23°58′30″N; longitude 84°2′–84°06′30″E) belongs to the western part of CGGC. It covers a vast area of about 100,000 km^2 and extends in the east–west from the provinces of Jharkhand, Orissa, Chhattisgarh, Madhya Pradesh and West Bengal and the south-eastern part of Uttar Pradesh. The CGGC includes multiple generations of mafic intrusives, namely meta-dolerite and norites to gabbros in which the corona texture is often demarcated at several places, especially in Purulia, Dumka and Daltonganj. This gneissic complex shows composite character consisting mainly of granitoid gneisses, migmatites and massive granites with enclaves of metasedimentary and meta-igneous rocks and intrusive basic and intermediate rocks (Ghose 1983, 1992; Chatterjee and Ghose 2011; Sanyal and Sengupta 2012; Yadav *et al.* 2016; Dwivedi *et al.* 2019 and references therein). The medium- to high-grade metamorphic terrain of CGGC mainly contains amphibolite to granulite facies rocks, which is sandwiched between the medium- to low-grade mobile belts. Here, the first one is located in the southern margin of CGGC and known as the North Singhbhum mobile belt, and it consists of the volcanic intrusive as well as sedimentary sequences (Saha 1994). The other mobile belt is located on the northern margin, and it extends from the north-western part of CGGC, which is called the Mahakoshal mobile belt. It preserves the metasediments, granitoids and mafic–ultramafic rocks (Roy and

Devarajan 2000). The CGGC has a broad history of two high-grade metamorphic events during the Mesoproterozoic and Grenvillian ages, and both these events recorded in the entire metamorphosed rock lie within CGGC (Pandey *et al.* 1986a, b; Ray Barman and Bishui 1994; Chatterjee *et al.* 2008; Maji *et al.* 2008; Sanyal and Sengupta 2012; Mukherjee *et al.* 2017). The north-western part of CGGC (Daltonganj) consists of granulite facies rocks, charnockite and migmatitic–tonalite–granodiorite–granite gneisses (Rode 1948; Dwivedi *et al.* 2019). The porphyritic granitic magmatism ($\sim$1660 ± 17 Ma) was reported from the western as well as the northern part of CGGC (Chatterjee and Ghose 2011; Saikia *et al.* 2017). The NE part of the CGGC is dominated by charnockitic gneisses as country rocks, and it was metamorphosed to amphibole–biotite gneiss. The 1447 ± 11 Ma age was obtained by U–Pb zircon dating from the protolith of the charnockitic gneisses and further high-grade metamorphism was recorded at 943 Ma from the migmatitic charnockitic gneiss under pressure–temperature (P–T) condition $\sim$9 kbar and 780–800°C (Mukherjee *et al.* 2017, 2018). Magmatic events are recorded from all parts of the CGGC during the Neoproterozoic era, which includes (a) partial melting and intrusive grey granite at 1005 ± 51 Ma and pink granite intrusion at 815 ± 47 Ma (Singh and Krishna 2009) and (b) granite intrusion emplaced at 975 Ma from Daltonganj of the western CGGC (Chatterjee and Ghose 2011). The geological map (figure 1a) represents the study area (Daltonganj) with geochronological age distribution at different locations within the CGGC, and the enlarged geological map of the study area is shown in figure 1(b).

3. Analytical techniques

The analytical work was performed using an EPMA on a CAMECA SX five instrument at the DST-SERB National Facility, Department of Geology (CAS), Institute of Science, BHU. The thin polished section was coated with a 20 nm thin layer of carbon for electron probe micro-analyses using a LEICA-EM ACE200 carbon coater instrument. The EPMA instrument CAMECA SX Five was operated with SX Five software at an accelerated voltage of 15 kV and a current of 200 nA with a LaB_6 source in the electron gun for electron beam generation, which is based on a new analytical protocol for the U–Th–Pb chemical dating of monazite (Pandey *et al.* 2019). Andradite is used as a natural silicate mineral to verify crystal positions by using an internal standard (SP2-LiF, SP3-LPET, SP4-LTAP and SP5-PET) with suitable wavelength dispersive spectrometers (SP#) using the CAMECA SX-Five instrument. The following X-ray lines were used in the analyses: F–Kα, Na–Kα, Mg–Kα, Al–Kα, Si–Kα, P–Kα, Cl–Kα, K–Kα, Ca–Kα, Ti–Kα, Cr–Kα, Mn–Kα, Fe–Kα, Ni–Kα and Ba–Lα. Natural mineral standards: fluorite, halite, periclase, corundum, wollastonite, apatite, orthoclase, rutile, chromite, rhodonite, hematite and barite; Ni pure metal standard was supplied by CAMECA-AMETEK which was used for routine calibration and quantification. Quantification of rare-earth element (REE) analysis in monazite mineral phases and U, Th and Y elemental X-ray mapping of monazite grains were obtained at an accelerating voltage of 20 kV, and currents of a beam are 200 nA, at 0.5 μm/pixel spatial resolution. The following X-ray lines were used in the analyses: Y–Lα, La–Lα, Ce–Lα, Pr–Lα, Nd–Lα, Sm–Lα, Eu–Lα, Th–Mα and U–Mα. All REE analysis was carried out on a LiF crystal attached with SP2 and Pb, Th and U were analysed with an LPET crystal connected with the SP3 spectrometer in a CAMECA-SX five EPMA instrument. Synthetic glass standards of all REE (La to U) supplied by CAMECA-AMETEK were used for routine calibration and quantification.

Scanning electron microscope (SEM) analysis was performed at the DST-SERB National Facility, Department of Geology (CAS), Institute of Science, BHU. The SEM instrument was operated at an accelerated voltage of 15 kV and a current of 200 nA.

4. Petrography and mineral chemistry

Different samples were collected from Datam and Mahawat Muria localities, which lie in the south-west of Daltonganj within CGGC (figure 1b). In this study, two rock samples (R-91-97 and R-91-96) were selected for the analytical purpose after the detailed petrographic study from collected rock samples. Representative mineral compositional data are presented in tables 2–6. The mineral

Table 1. *Four metamorphic (M_1–M_4) stages with geochronology from different localities of the CGGC (modified after Sanyal and Sengupta 2012).*

Age (Ma)	Type of metamorphism	Dating technique	Type of rocks	Locality	Authors
M_1 (Palaeo-proterozoic)					
1.870–1.691; Mnz core	UHT metamorphism	U–Th–Pb monazite	Khondalite enclaves	Southern CGGC margin	Chatterjee *et al.* (2010)
1824–1659; Mnz core Gt hosted 1720 ± 31; Mnz core	HP (9–12 kbar) and MT (730–800°C)		Migmatitic quartzo-feldspathic gneiss Metapelitic granulite	NE of Dumka near the northern CGGC margin	Chatterjee *et al.* (2010)
1741 ± 65	UHT metamorphism	Rb–Sr whole-rock isochron age dating	Granite	NW CGGC	Ray Barman and Bishui (1994)
1700–1650	UHT metamorphism (sulphide mineralisation)	Pb–Pb mineral age dating	Galena from sulphide-bearing metasediments	Hesatu–Belbathan area	Singh *et al.* (2001)
1697 ± 17 1583 ± 50	Retrograde metamorphism	U–Th–Pb monazite U–Th–Pb xenotime	Porphyritic granite	NW CGGC	Chatterjee and Ghose (2011)
M_2 (Palaeo- to Mesoproterozoic)					
1628: Mnz core 1518: Mnz core	UHT metamorphism (5–6 kbar/930–950°C)	U–Th–Pb monazite	Quartzo-feldspathic granulite and khondalite	East of Trikut Pahar near Deoghar	Sanyal *et al.* (2007)
1624 ± 5, 1000 1515 ± 5, 1000 1515	Isobaric cooling (IBC) path	Rb–Sr whole rock isochron age dating	Hy-granite gneiss Massive charnockite Basic granulite	Jamua–Dumka	Ray Barman *et al.* (1994)
1599–1522	UHT metamorphism	Rb–Sr whole rock isochron age dating	Felsic gneiss	Mor Valley	Mallik *et al.* (1991)
1550 ± 12	UHT metamorphism	U–Pb zircon (ID-TIMS)	Gabbroic anorthosite	Saltora (West Bengal)	Chatterjee *et al.* (2008)
1457 ± 63	IBC path	Rb–Sr whole rock isochron age dating	Charnockite gneiss	Jamua–Dumka	Ray Barman *et al.* (1994)
1331 ± 125 1465 ± 17 1447 ± 11	Isothermal decompression (ITD)	U–Pb zircon (LA-ICP-MS)	Syenite Ferroan granitoid A-Type granitoid	Between Dumka and Deoghar	Mukherjee *et al.* (2017, 2018)
1442–1305: Mnz core 1272 ± 35: Mnz core	Prograde metamorphism	U–Th–Pb monazite	Granite gneiss Porphyritic granite	Southern CGGC NE of Dumka	Chatterjee *et al.* (2010)
1416–1246	UHT metamorphism	K–Ar whole rock age dating	Migmatitic granite gneiss	NE part of the CGGC	Sarkar (1980)
1300–1110	UHT metamorphism (intrusive granite)	Rb–Sr whole rock isochronage dating	Migmatitic granite gneiss	Hesatu–Belbathan area	Pandey *et al.* (1986a, b)
M_3 (Meso- to Neoproterozoic)					
1190 ± 26: Mnz rim Gt 995 ± 24: Mnz rim Gt 950 ± 20: Mnz in matrix	Prograde metamorphism (7–10.5 kb/775–825°C)	U–Th–Pb monazite	Metapelitic granulite	NW of Dumka	Chatterjee *et al.* (2008)
947 ± 27	High-grade metamorphism (8.5–11 kb/50–900°C)	U–Pb zircon (ID-TIMS) technique	Gabbroic anorthosite	Saltora (West Bengal)	Chatterjee *et al.* (2008)

1178 ± 61	ITD path	Rb–Sr whole rock isochron age dating	Migmatitic granite gneiss	Jamua–Dumka	Ray Barman *et al.* (1994)
1071 ± 64			Porphyritic granite	Bero–NE Purulia	
1176 ± 9: Mnz in Gt 1082 ± 9: Mnz in Matrix 1041 ± 20: Mnz in Gt 981 ± 26: Mnz in matrix	Prograde metamorphism (750–850°C/4–6 kbar)	U–Th–Pb monazite	Garnetiferous metapelitic gneiss	Bero–Saltora (WB)	Maji *et al.* (2008)
1021 ± 26: Mnz in Gt 992 ± 11: Mnz in matrix 977 ± 15: Mnz in Gt 967 ± 11: Mnz in matrix	Prograde metamorphism	U–Th–Pb monazite	Foliated granite	Bero–Saltora (WB)	Maji *et al.* (2008)
1118 & 1088: Mnz outer core in matrix 979 & 942: Mnz rim in quartzose matrix		U–Th–Pb monazite	Quartzo-feldspathic granulite and khondalite	East of Trikut Pahar near Deoghar	Sanyal *et al.* (2007)
1086–850		K–Ar whole-rock dating	Porphyritic granite gneiss	Near Ranchi–Muri	Sarkar (1980)
1005 ± 51	UHT metamorphism	Rb–Sr whole-rock dating	Grey granite gneiss	Raikera–Kunkuri, Jashpur (Chhattisgarh)	Singh and Krishna (2009)
990–940	ITD path (11 to 5 kbar)	U–Th–Pb monazite	Basic granulites	Bero–NE Purulia	Karmakar *et al.* (2011)
984–930: Mnz in Gt and matrix	ITD	U–Th–Pb monazite	Migmatitic quartzo-feldspathic gneiss	NE of Dumka near the northern CGGC margin	Chatterjee *et al.* (2010)
954 ± 32: Mnz rim			Porphyritic granite		
940–924: Mnz rim			Metapelitic granulite		
967–939: Mnz core	Retrogression metamorphism	U–Th–Pb monazite	Granite gneiss	Near the southern CGGC margin	Chatterjee *et al.* (2010)
965 ± 51: Mnz rim			Porphyritic granite		
937 ± 30			Metapelitic granulite		
975 ± 67	High-grade prograde metamorphism	U–Th–Pb monazite	Pink granite	NW CGGC	Chatterjee and Ghose (2011)
948 ± 22 943	Prograde metamorphism until peak (high pressure)	U–Pb zircon (LA-ICP-MS)	Amp-Bt-gneiss Charnockitic gneiss	Between Dumka and Deoghar	Mukherjee *et al.* (2017, 2018)
M_4 (Neoproterozoic)					
876–828; Mnz in Gt and matrix	Retrogression metamorphism	U–Th–Pb monazite	Migmatitic quartzo-feldspathic gneiss	NE of Dumka, northern CGC margin	Chatterjee *et al.* (2010)
859 ± 87: Mnz rim			Granite gneiss	Near the southern CGGC margin	
778–860: Mnz core-rim			Porphyritic granite		
862: Mnz in biotite 842: Mnz in biotite 788: Mnz rim in quartzose matrix		U–Th–Pb monazite	Quartzo-feldspathic granulite and khondalite	East of Trikut Pahar near Deoghar	Sanyal *et al.* (2007)
825 ± 26: Mnz in Gt 818 ± 11: Mnz in matrix	Prograde metamorphism (650 ± 50°C/4–5 kbar)	U–Th–Pb monazite	Garnetiferous metapelitic gneiss	Bero–Saltora (WB)	Maji *et al.* (2008)
815 ± 47	Metasomatism	Rb–Sr whole rock	Pink granite	Raikera–Kunkuri, Jashpur (Chhattisgarh)	Singh and Krishna (2009)

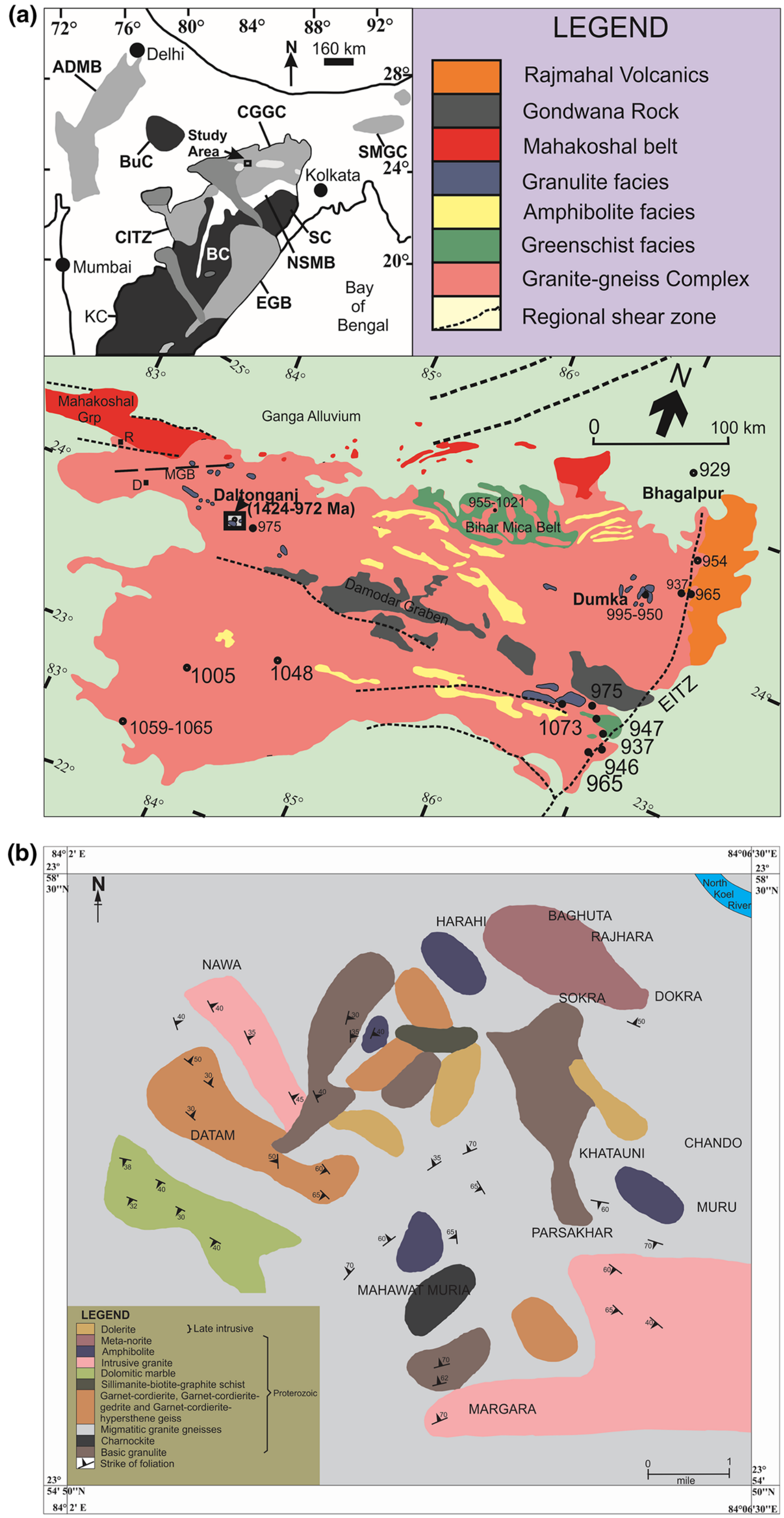

Figure 1. (**a**) Geological map of the CGGC (modified after Acharyya 2003; Maji *et al.* 2008; Chatterjee and Ghose 2011). Abbreviations: ADMB: Aravalli–Delhi mobile belt, BC: Bastar craton, BuC: Bundelkhand craton, CGGC: Chhotanagpur granite gneiss complex, CITZ: Central Indian tectonic zone, D: Dudhi, DM: Dumka, EGB: Eastern Ghats belt, KC: Karnataka craton, MGB: Makrohar granulite belt, NSMB: North Singhbhum mobile belt, R: Rihand–Renusagar area, SC: Singhbhum craton and SMGC: Shillong–Meghalaya gneissic complex. Here, the distribution of different geochronological (Grenvillian) ages in different locations, with our analysed monazite dating age is 1424–972 Ma from the Daltonganj (CGGC) India. (**b**) Enlarged geological map of the area around the south-west of Daltonganj, Palamau (Jharkhand) district, India.

Table 2. *Representative electron microprobe analyses and structural formula of garnet and hypersthene.*

	Garnet				Hypersthene		
	Sample no. R-91-97		Sample no. R-91-96		Sample no. R-91-97		
Domain	122/45	122/20	122/44	122/46	80/1	155/1	146/1
SiO_2	37.650	36.558	37.397	37.610	48.272	52.127	52.874
TiO_2	0.005	0.002	0.005	0.011			
Al_2O_3	20.194	20.458	20.369	20.367	3.424	3.798	3.291
FeO	34.388	35.823	34.355	34.388	28.901	23.976	23.174
MnO	0.302	0.336	0.481	0.223			
MgO	7.278	6.797	7.256	7.104	17.315	18.329	18.164
CaO	0.260	0.239	0.254	0.247	0.044	0.054	0.054
Na_2O	0.009	0.002	0.009	0.023	0.007	0.568	0.490
K_2O	0.023	0.02	0.019	0.014			
Total	**100.109**	**100.234**	**100.143**	**99.986**	**98.151**	**98.852**	**98.371**
Si	2.963	2.886	2.942	2.965	1.897	1.968	2.000
Al^{iv}	0.000	0.000	0.000	0.000	0.103	0.032	0.000
ΣZ	2.963	2.886	2.942	2.965	2	2	2
Al^{vi}	1.874	1.904	1.889	1.893	0.056	0.137	0.148
Ti	0.001	0	0.001	0.001			
Fe^{3+}	0.203	0.326	0.229	0.180	0.070	0.000	0.000
ΣY	2.078	2.23	2.119	2.074			
Fe^{2+}	2.081	2.039	2.031	2.087	0.875	0.763	0.744
Mn	0.020	0.023	0.032	0.015			
Mg	0.864	0.8	0.851	0.834	1.015	1.031	1.025
Ca	0.022	0.02	0.021	0.021	0.002	0.002	0.002
Na	0.002	0	0.002	0.003	0.001	0.042	0.036
K	0.002	0.002	0.002	0.001			
ΣX	2.991	2.884	2.939	2.961	2.018	1.975	1.954
X_{Mg}	0.274	0.253	0.274	0.269	0.52	0.57	0.58
Pyrope	28.90	27.74	28.96	28.17			
Almandine	69.69	70.7	69.11	70.48			
Grossularite	0.74	0.69	0.72	0.71			
Spessartite	0.67	0.8	1.09	0.51			

X_{Mg} = Mg/(Mg + Fe). Structural formula of garnet based on 12 oxygen basis and hypersthene based on six oxygen basis.

abbreviations used in this study are after Whitney and Evans (2010).

4.1 *Megascopic characters*

The R-91-97 contains garnet–hypersthene–gedrite–cordierite gneisses, and R-91-96 consists of garnet–gedrite–cordierite–biotite gneisses, which are medium- to coarse-grained and exhibit gneissose texture with a resinous and greasy appearance. The garnet–gedrite–cordierite–biotite gneiss consists of garnet as one of their dominant minerals displaying light pinkish colour with the dark-coloured gedrite along with biotite flakes (figure 2a). Garnet–hypersthene–gedrite–cordierite gneiss contains the porphyroblastic garnet with medium- to small-size grains of hypersthene, gedrite, cordierite, biotite and quartz (figure 2b). The presence of garnet has displayed pinkish to reddish tinge to the rock. On the weathered surface of such gneisses, the nodules of garnet are generally seen on the rock surface in the hand-specimen. The detail petrography and reaction texture of these rocks were discussed by Dwivedi *et al.* (2019).

4.2 *Identification of monazite*

Monazite occurs as an accessory phase in the rocks of the study area. In the context of the identification of monazite grain under a petrological microscope, zircon creates some confusion with monazite. Monazite and zircon have some vital diagnostic features, and they could be distinguished by their characteristic. The zircon grains have distinct prismatic as well as

Table 3. *Representative electron microprobe analyses and structural formula of gedrite and cordierite.*

	Gedrite				Cordierite			
	Sample no. R-91-97		Sample no. R-91-96		Sample no. R-91-97		Sample no. R-91-96	
Domain	174/1	176/1	86/1	87/1	24/1	25/1	120/1	139/1
SiO_2	49.813	44.912	45.674	46.39	48.937	49.241	48.695	49.536
TiO_2	0.017	0.256	0.222	0				
Al_2O_3	6.39	11.83	11.523	10.24	30.111	30.457	30.222	30.381
FeO	22.039	22.525	21.718	21.407	5.865	5.564	6.240	5.330
MgO	16.986	14.979	15.569	16.19	10.204	10.024	9.926	10.168
CaO	0.081	0.095	0.052	0.075				
Na_2O	0.793	1.613	1.61	1.307	0.156	0.141	0.148	0.102
BaO	0.305	0.339	0.204	0.238				
F	0.275	0.223	0.341	0.369				
Total	**96.762**	**96.876**	**96.938**	**96.226**	**95.273**	**95.426**	**95.232**	**95.518**
Si	7.36	6.704	6.772	6.912	5.140	5.151	5.127	5.169
Al^{iv}	0.64	1.296	1.228	1.088	3.727	3.755	3.750	3.736
ΣZ	8	8	8	8	8.867	8.907	8.876	8.905
Al^{vi}	0.472	0.785	0.786	0.71				
Ti	0.002	0.029	0.025	0				
Fe^{2+}	2.723	2.812	2.693	2.667	0.548	0.487	0.549	0.465
Mg	3.741	3.333	3.441	3.596	1.598	1.563	1.558	1.582
ΣX	6.938	6.959	6.945	6.974	2.146	2.050	2.107	2.047
Ca	0.013	0.015	0.008	0.012				
Na	0.227	0.467	0.463	0.378	0.032	0.028	0.030	0.021
Ba	0.017	0.02	0.012	0.014				
ΣY	0.258	0.502	0.483	0.403				
F	0.128	0.105	0.16	0.174				
OH*	1.872	1.895	1.84	1.826				
X_{Mg}	0.58	0.54	0.56	0.57	0.745	0.762	0.739	0.773

X_{Mg} = Mg/(Mg + Fe). Structural formula calculation of gedrite based on 23 oxygen basis and cordierite based on 18 oxygen basis.

*: Calculated values.

euhedral shape, but monazite grains are rarely rounded and anhedral in shape (Schaltegger *et al.* 1999). The pleochroic haloes formed by zircons were small, but monazite produced comparatively larger pleochroic haloes in flakes of biotite and cordierite, due to an abundance of Th, i.e., 3.14–7.20 wt%. However, solely on optical properties, monazite and zircon grains cannot be easily distinguished. The back-scattered electron (BSE) images were used to identify the monazite grains from the matrix and garnet.

4.3 *Textural interpretations of monazite*

The analyzed monazite grains occur as inclusion within porphyroblastic garnet, cordierite biotite and matrix (figure 3). Garnet shows the compositional variation from the core to the rim in which the core ($Py_{29.5}Alm_{69.5}Grs_{0.7}Sps_{0.3}$) contains comparatively lower Alm and Sps and slightly higher in pyrope content in comparison with the rim ($Py_{23.3}Alm_{75.4}$-$Grs_{0.6}Sps_{0.7}$) (figure 4). Monazite grain in the core of garnet (figure 3a) produced the older age in R-91-97, and many of the monazite grains embedded in the periphery area (figure 3b) generates the younger age in R-91-96. Garnet is rimmed by cordierite and shows the corona structure (figure 3a) which includes biotite and quartz as inclusion that leads to the formation of cordierite. Monazite grains are also present in the cordierite, biotite (figure 3c and d), gedrite and matrix which provide a younger age.

4.4 *Microscopic characters and mineral chemistry*

Garnet occurs as coarse xenoblast and poikiloblast and contains gedrite, cordierite, biotite and quartz as

Table 4. *Representative electron microprobe analyses and structural formula of biotite.*

	Sample no. R-91-97		Sample no. R-91-96		
Domain	159/1	163/1	52/1	164/1	158/1
SiO_2	39.067	38.778	38.377	37.884	38.573
TiO_2	1.675	1.712	1.738	1.624	1.993
Al_2O_3	14.372	14.967	14.970	14.480	14.571
FeO	13.072	12.707	11.619	12.407	12.043
MgO	18.113	17.504	17.713	17.214	17.506
CaO	0.028	0.000	0.000	0.001	0.004
BaO	0.242	0.000	0.000	0.104	0.000
Na_2O	0.513	0.635	0.626	0.618	0.669
K_2O	8.019	8.984	8.796	9.160	8.969
Cl	0.055	0.041	0.000	0.050	0.050
F	1.696	2.112	1.775	2.052	2.122
Total	**96.853**	**97.441**	**95.766**	**95.595**	**96.498**
Si	5.738	5.699	5.698	5.694	5.715
Al^{iv}	2.262	2.301	2.302	2.306	2.285
ΣZ	8	8	8	8	8
Al^{vi}	0.226	0.292	0.318	0.259	0.259
Ti	0.185	0.189	0.194	0.184	0.222
Fe^{2+}	1.606	1.562	1.443	1.559	1.492
Ba	0.014	0.000	0.000	0.006	0.000
Mg	3.966	3.835	3.921	3.857	3.867
ΣX	5.997	5.878	5.875	5.865	5.840
Ca	0.004	0.000	0.000	0.000	0.001
Na	0.146	0.181	0.180	0.180	0.192
K	1.503	1.684	1.666	1.756	1.695
ΣY	1.653	1.865	1.846	1.936	1.888
Cl	0.014	0.010	0.000	0.013	0.012
F	0.788	0.982	0.833	0.975	0.994
X_{Mg}	0.71	0.71	0.73	0.71	0.72

X_{Mg} = Mg/(Mg + Fe). Structural formula calculated on 22 oxygen basis.

Table 5. *Representative electron microprobe analyses and structural formula of ilmenite.*

	Sample no. R-91-97		Sample no. R-91-96		
Domain	34/1	35/1	36/1	45/1	46/1
TiO_2	51.496	51.342	50.488	50.133	49.759
FeO	46.442	47.991	47.860	47.856	48.121
MnO	0.221	0.312	0.412	0.235	0.312
MgO	0.734	0.049	0.135	0.106	0.061
SiO_2	0.132	0.025	0.136	0.019	0.1
Total	**99.025**	**99.719**	**99.030**	**98.348**	**98.353**
Ti	0.886	0.891	0.864	0.873	0.846
Fe^{3+}	0.090	0.087	0.065	0.087	0.069
Fe^{2+}	0.924	0.935	0.986	0.946	0.965
Mn	0.012	0.017	0.024	0.004	0.018
Mg	0.026	0.001	0.012	0.004	0.001
Si	0.007	0.001	0.011	0.001	0.008
Total	**1.945**	**1.932**	**1.962**	**1.915**	**1.907**

Structural formula calculated on three oxygen basis.

an inclusion with some other heavy minerals i.e., monazite, ilmenite, magnetite, zircon, etc. Garnet grains are highly fractured and partially rimmed by gedrite and cordierite. The small flake of biotite occurs as inclusion along with quartz within the garnet (figure 2c). Garnet shows solid solution dominantly between almandine (65.4–74.3 mol%) and pyrope (24.3–32.8 mol%) with minor amounts of grossular (0.7–1.2 mol%) and spessartine (0.6–0.7 mol%). The X_{Mg} of garnet lies between 0.25 and 0.27 (table 2).

The BSE image shows the inclusion of biotite and quartz in garnet (figure 4a), and the elemental X-ray map of garnet reveals the enrichment of Fe and Mg elements (figure 4b and c) and depletion of Mn and Ca elements (figure 4d and e). Garnet shows the dominance of the almandine in which X_{Alm} varies from 0.68 to 0.77. The length of the porphyroblastic garnet is 890 μm, and the rim–core–rim distribution of almandine and pyrope garnet is graphically represented (figure 4f). Here almandine shows a high-composition peak at the rim and a lower one at the core area. Pyrope represents a higher occurrence at the core and lower occurrence at the rim portion (X_{Py} = 0.22–0.34). The Fe content of garnet increases and the Mg content decreases at the rim of the garnet porphyroblast due to locally resorbed by gedrite + cordierite minerals or by retrogressive biotite. This situation indicates the lowering of the pressure and the temperature at the rim of garnet porphyroblast as compared to the core portion.

Hypersthene is idioblastic to xenoblastic in nature and varies from medium to coarse (figure 2c). It shows strong pleochroism from pink to bluish-green in colour. Hypersthene is partially rimmed by garnet and gedrite. The X_{Mg} of hypersthene ranges between 0.52 and 0.58 (table 2).

Xenoblast and coarse aggregates of cordierite wrap the garnet and gedrite (figure 2d). Corroded cordierite is completely rimmed by garnet which provides evidence of the prograde metamorphic condition. Cordierite shows some alteration along the grain boundaries and the fractured zone. Cordierite includes magnetite, quartz, monazite, etc. as inclusions. Cordierite compositions are magnesian, and X_{Mg} ranges from 0.74 to 0.77 (table 3).

Gedrite is coarse-grained and has idioblastic prisms in thin sections. It is commonly associated with biotite to define foliation in rocks (figure 2d).

Table 6. *Representative electron microprobe analyses and structural formula of monazite.*

	Sample no. R-91-97						Sample no. R-91-96					
Domain	8/2	10/2	11/2	12/2	13/2	14/2	1/2	2/2	3/2	4/2	5/2	7/2
SiO_2	0.625	0.815	0.486	0.409	0.635	0.434	0.337	0.495	0.266	0.577	0.537	0.266
P_2O_5	30.941	29.938	29.907	30.351	30.365	30.583	30.255	29.495	30.509	29.617	30.210	30.509
CaO	0.840	1.188	0.665	1.108	1.128	1.136	0.916	0.899	0.663	0.840	1.027	0.663
Y_2O_3	1.456	1.408	2.042	1.446	1.406	1.648	0.914	1.0676	0.808	1.025	1.162	0.808
La_2O_3	16.125	15.888	15.322	15.446	15.491	15.350	15.692	15.931	16.568	15.430	15.722	16.568
Ce_2O_3	27.629	27.354	26.854	26.265	27.257	26.512	28.866	27.217	28.270	28.564	27.485	28.270
Pr_2O_3	3.135	2.877	3.188	3.117	2.961	3.028	3.311	3.230	3.302	3.088	3.260	3.302
Nd_2O_3	9.910	10.690	10.470	10.330	10.964	11.230	10.466	10.326	10.556	11.023	10.447	10.556
Sm_2O_3	1.850	1.767	1.494	1.670	1.518	1.540	1.808	1.838	1.895	1.836	1.808	1.895
Eu_2O_3	1.320	1.323	1.198	1.441	1.430	1.429	1.466	1.491	1.432	1.393	1.429	1.432
Gd_2O_3	1.262	1.350	1.193	1.265	1.038	1.216	1.181	1.309	1.175	1.272	0.98	1.175
PbO	0.261	0.440	0.423	0.442	0.394	0.419	0.316	0.463	0.361	0.258	0.434	0.361
ThO_2	3.526	4.355	5.690	5.510	4.747	5.054	3.921	4.796	3.707	3.516	4.794	4.569
UO_2	0.280	0.674	0.348	0.376	0.564	0.431	0.258	0.779	0.390	0.279	0.772	0.390
Total	**99.158**	**100.068**	**99.280**	**99.175**	**99.898**	**100.009**	**99.703**	**99.337**	**99.903**	**98.719**	**100.075**	**100.764**
Si	0.026	0.037	0.019	0.016	0.026	0.02	0.014	0.018	0.01	0.024	0.02	0.011
P	1.007	0.996	1.001	1.007	1.007	1.001	1.005	1.001	1.008	0.99	1.005	1.007
Ca	0.036	0.049	0.028	0.042	0.043	0.043	0.038	0.036	0.028	0.036	0.04	0.028
Y	0.03	0.031	0.048	0.03	0.029	0.026	0.019	0.023	0.015	0.024	0.028	0.014
La	0.232	0.231	0.222	0.224	0.226	0.224	0.226	0.228	0.232	0.223	0.227	0.248
Ce	0.396	0.384	0.384	0.381	0.381	0.389	0.4	0.396	0.412	0.403	0.396	0.414
Pr	0.045	0.039	0.045	0.043	0.041	0.039	0.047	0.045	0.047	0.043	0.047	0.047
Nd	0.142	0.148	0.146	0.143	0.155	0.151	0.146	0.144	0.144	0.157	0.144	0.144
Sm	0.024	0.022	0.021	0.022	0.02	0.018	0.023	0.022	0.025	0.024	0.025	0.024
Eu	0.02	0.017	0.017	0.018	0.02	0.021	0.019	0.021	0.018	0.019	0.018	0.02
Gd	0.014	0.016	0.012	0.014	0.012	0.011	0.014	0.019	0.014	0.014	0.012	0.012
Pb	0.002	0.003	0.003	0.003	0.003	0.003	0.002	0.003	0.003	0.002	0.003	0.003
Th	0.031	0.044	0.049	0.047	0.04	0.038	0.04	0.05	0.04	0.031	0.04	0.048
UO_2	0.005	0.007	0.005	0.005	0.005	0.007	0.003	0.008	0.004	0.003	0.009	0.005
Total	**2.01**	**2.023**	**2.000**	**1.995**	**2.008**	**1.991**	**1.996**	**2.014**	**2.000**	**1.993**	**2.014**	**2.025**

Structural formula calculated on four oxygen basis, in ion per formula unit; 0.00 values indicate the below detection limit.

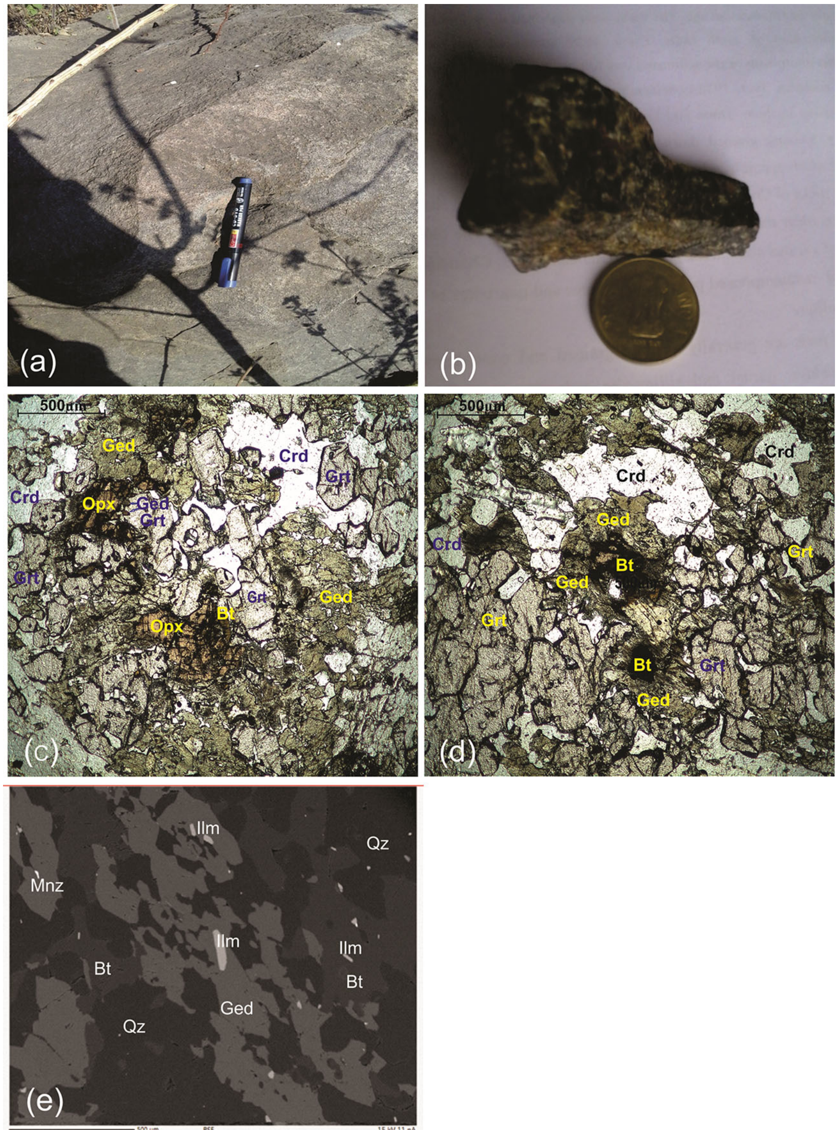

Figure 2. (**a**) Field photograph of the garnet–gedrite–cordierite–biotite gneiss; (**b**) representative hand-specimen of the garnet–orthopyroxene–gedrite–cordierite gneiss; (**c**) photomicrographs showing the gedrite rimmed by garnet and cordierite, where orthopyroxene coexists with garnet; (**d**) photomicrographs showing the small grain of brown biotite present as inclusion in gedrite and gedrites are surrounded by a huge mass of garnet and cordierite; (**e**) BSE image shows some accessory minerals, i.e., monazite and ilmenite with other minerals like gedrite, biotite and quartz.

It contains inclusions of cordierite, biotite, quartz, etc. It shows parallel extinction and pleochroism in which the colour varies from yellowish green to greenish brown. Gedrite contains a trail of biotite as inclusion which suggests the appearance of gedrite in the rock due to the breakdown of biotite + quartz. Gedrite consists of Al^{IV} and Al^{VI} components in sufficient quantities 0.64–1.29 and 0.47–0.78 pfu, respectively, and the X_{Mg} ranges from 0.54 to 0.58 (table 3).

Biotite occurs in the form of small flakes and as individual laths within the hypersthene (figure 2c). It occurs as inclusion in gedrite and partially wrapped by cordierite (figure 2d). The TiO_2 content of biotite varies from 1.62 to 1.99 wt%, and its compositions are magnesian with the X_{Mg} ranges from 0.71 to 0.73 (table 4).

Ilmenite occurs as elongated and prismatic grains, which are very fine-grained and present as inclusion in gedrite, biotite, garnet and other mineral grains (figure 2e). Compositionally, they are magnesian–mangaon ilmenites (MgO: 0.049–0.734 wt% and MnO: 0.221–0.412 wt%) (table 5).

Monazite grains occur as accessory minerals in the matrix and are ubiquitous in garnet–hypersthene–gedrite–cordierite gneisses as well as

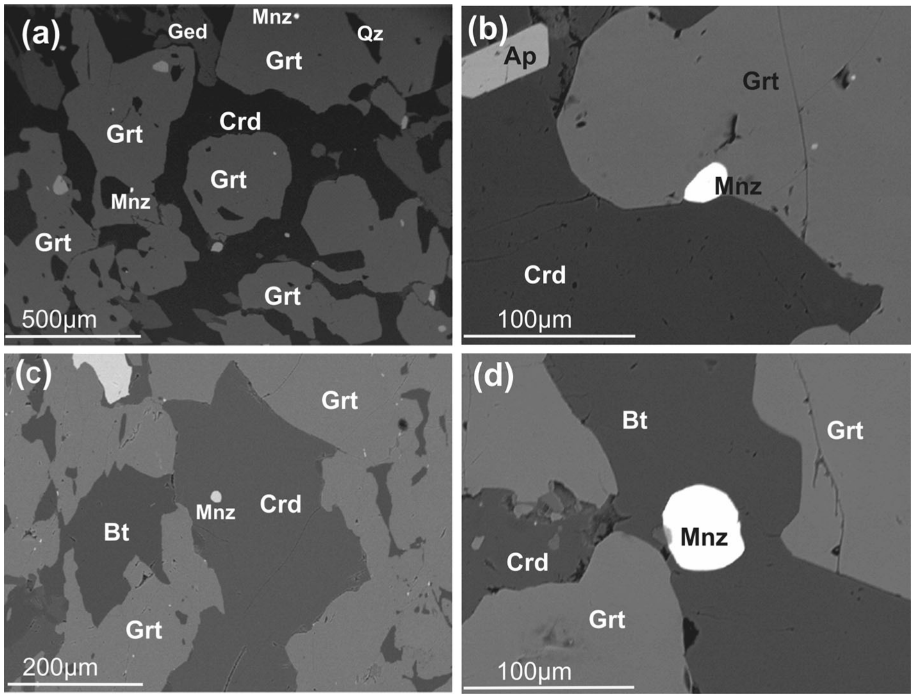

Figure 3. BSE images showing the microstructural and textural settings of monazite occurrences in the granulitic gneiss of Daltonganj. (**a**) Monazite occurring as inclusion within porphyroblastic garnet in R-91-97. (**b**) Monazite grain occurring as inclusion within the periphery area of garnet in R-91-97. (**c**) Monazite present as inclusion in the cordierite, Crd are later surrounded by garnet in R-91-96. (**d**) Monazite occurring as inclusion within biotite in R-91-96.

garnet–gedrite–cordierite–biotite gneisses; large grains of monazite (60–80 micron) are commonly found in high-grade metamorphic rocks (Montel *et al.* 1996). The monazite grains contain 3.14–7.20 wt% of thorium oxide (ThO_2), 0.28–1.52 wt% of uranium oxide (UO_2) and 0.26–0.44 wt% of lead oxide (PbO) in the sample R-91-97. The sample R-91-96 contains 3.53–6.18 wt% of ThO_2, 0.26–1.45 wt% of UO_2 and 0.26–0.46 wt% of (PbO). The normalised cations based on the four oxygen basis are presented in table 6 and supplementary table 1.

5. Monazite geochronology

5.1 *Sample description and U–Th–Pb systematics*

R-91-97 and R-91-96 samples have been chosen for microprobe dating after systematic EPMA-BSE imaging. Monazite grains are of diameter (70–80 μm) and compositionally homogeneous (figure 5a–h). The monazite grains show the homogeneous compositional domain which is demarcated by the BSE image and X-ray elemental mapping. The X-ray elemental maps of some selective monazite grains P43 of R-91-97 and P46 of R-91-96 are shown in figure 5(a–h). Both P43 and P46 monazite grains occur as inclusions in the garnet porphyroblast and are relatively poor in yttrium (Y) elemental composition at the outer rim margin in comparison with the core (figure 5d and h). The yttrium (Y) partitioning in the monazite is directly linked to the growth or consumption by the peritectic garnet (Spear and Pyle 2010; Bhowmik *et al.* 2014). But, U and Th X-ray elemental maps are showing homogeneous composition in both the grains (figure 5b, c, f and g). U and Th with Pb were found to occur together in both huttonite and brabantite types of substitution. Monazite shows the compositional variation between Th (+Ca and Si) and Y (+HREE) and it reflects the different substitutions: brabantite substitution ($Th^{4+} + Ca^{2+} = 2REE^{3+}$; Rose 1980) and huttonite substitution ($Th^{4+} + Si^{4+} = LREE^{3+} + P^{5+}$; Pabst and Hutton 1951). The variation of the brabantite *vs.* huttonite exchange operation is presented in the plot of Th + U + Si *vs.* REE + Y + P (figure 6). All monazite grains contained negligible SiO_2. However, they contain sufficient amounts of Ca which quantify the brabantite (Th/U + Ca ↔ 2REE) substitution. Here, the brabantite substitution is dominant in monazites.

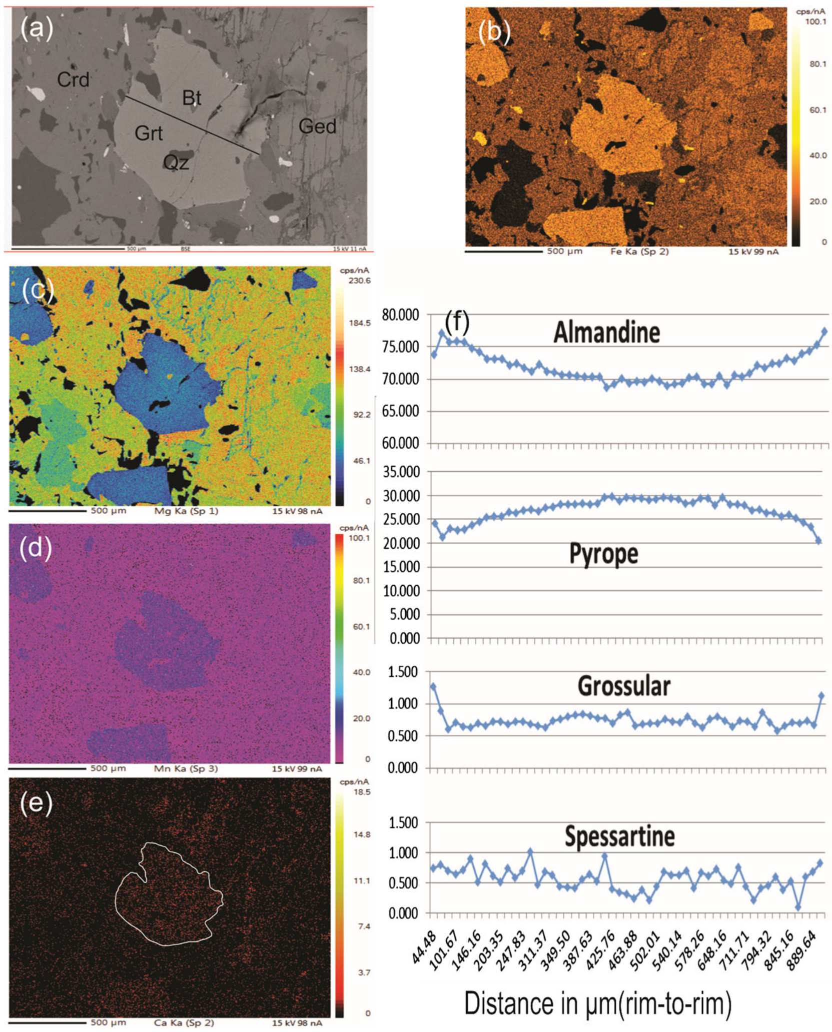

Figure 4. (**a**) BSE image of garnet porphyroblast with inclusions of biotite and quartz; (**b–e**) these images represent the X-ray mapping of Fe, Mg, Mn and Ca in garnet porphyroblast; (**f**) X_{Alm}, X_{Py}, X_{Grs} and X_{Sps} variation along the garnet porphyroblast from rim to rim.

5.2 *Electron microprobe dating*

Electron microprobe dating can be used as an efficient investigation tool for finding the age of metamorphism and deformational history (Williams *et al.* 1999). Here, EPMA monazite geochronology was conducted to find out the age, and to establish the evolutionary history of the granulite of Daltonganj.

Monazite grains vary in shape from anhedral to subhedral or rounded and size from the smaller grain (10–30 µm) to larger grain (60–80 µm). It occurs as inclusion within garnet and the matrix. Estimation of age and uncertainties are compared from different monazite grains, and monazite growth events were interpreted which recorded from the Daltonganj area of CGGC. A total of 39 EPMA ages were obtained from 39 monazite mineral grains of the two different granulite samples. The Th–U–Pb values from the different monazite grains of R-91-97 and R-91-96 samples are given in table 7. EPMA dating generates two age domains, and the calculated monazite ages range from 1348 ± 47 to 1482 ± 49 Ma and 896 ± 49 to 1050 ± 63 Ma in R-91-97, and vary from 1322 ± 64 to 1494 ± 65 Ma and 926 ± 58 to 1019 ± 59 Ma in R-91-96 (figure 7). The weighted average age distribution and probability density plot was obtained by using the ISOPLOT program (Ludwig 2011) which is depicted in figure 8a–h. The analysis of sample R-91-97 produced age population at 1424 ± 64 Ma (figure 8a and b) and 972 ± 28 Ma, with 95% confidence (figure 8c and d). The sample R-91-96 yielded age population at 1390 ± 56 Ma (figure 8e and f) and 962 ± 159 Ma, with 95% confidence (figure 8g and h). The electron microprobe dating of monazite grains has generated the two-age domain from both rocks, i.e., garnet–hypersthene–gedrite–cordierite gneiss and

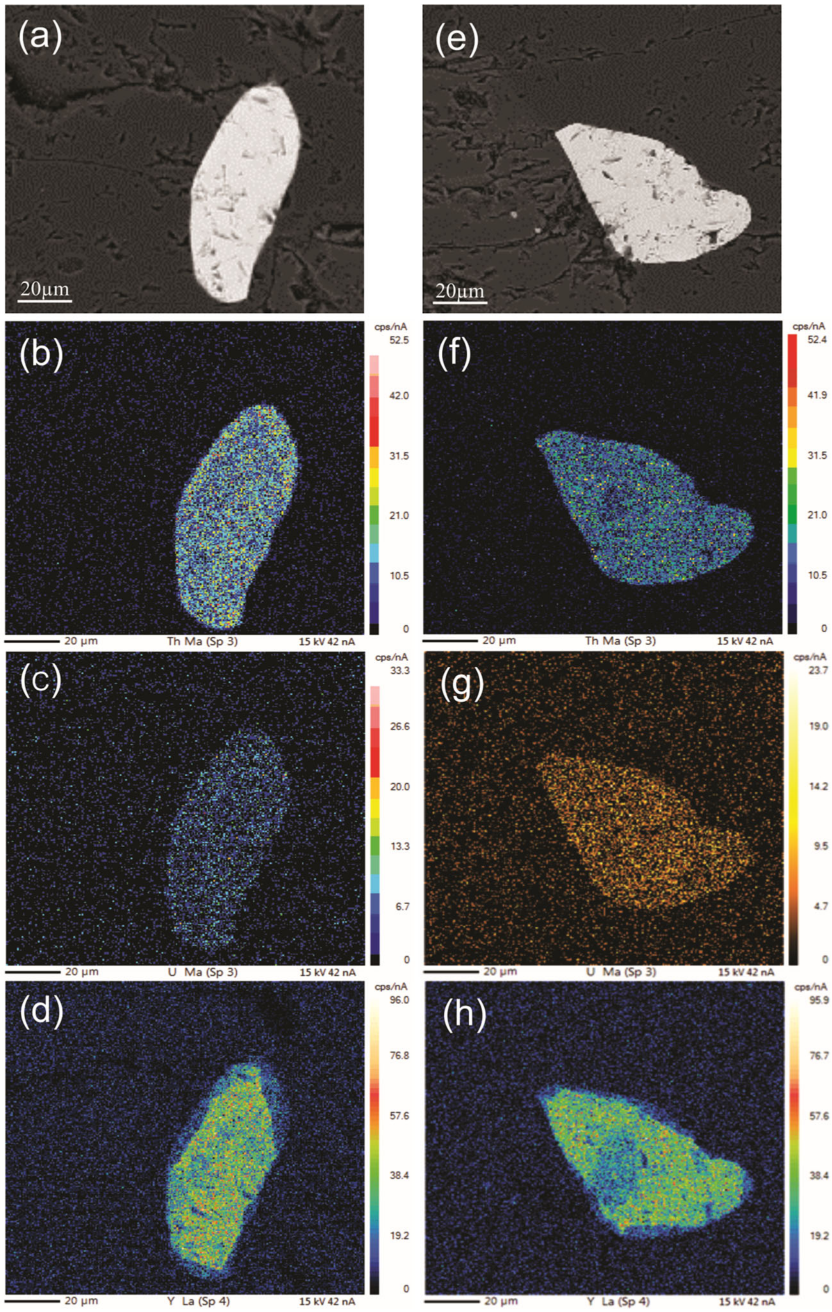

Figure 5. Grain-P43 of the R-91-97 sample, (**a**) BSE image. (**b**) and (**c**) X-ray elemental maps documenting the homogeneous pattern of Th and U elements in monazite. (**d**) X-ray map shows the zoning pattern at the outer part in monazite; wherein grain-P46 of the R-91-96 sample, (**e**) BSE image, (**f**) and (**g**) X-ray elemental maps documenting the homogeneous pattern of Th and U elements in the monazite. (**h**) X-ray map shows the zoning pattern at the outer part as well as the core of monazite.

garnet–gedrite–cordierite–biotite gneiss, which lies around the Mesoproterozoic and Grenville orogeny age.

6. *P–T* condition of metamorphism

The *P–T* conditions were estimated from the heterogeneous compositions of garnet and cordierite from garnet–hypersthene–gedrite–cordierite gneiss. The garnet–cordierite Mg–Fe exchange geothermometers and garnet–cordierite–sillimanite–quartz geobarometers were used to estimate the *P–T* conditions and their results are summarised in tables 8 and 9. The maximum and minimum temperatures obtained at 7 kbar pressure were 788° and 656°C, respectively. At 700°C, the corresponding pressure varies from 4.80 to 7.34 kbar. By using the THERMOCALC v-3.21 thermodynamic modelling program by Holland and

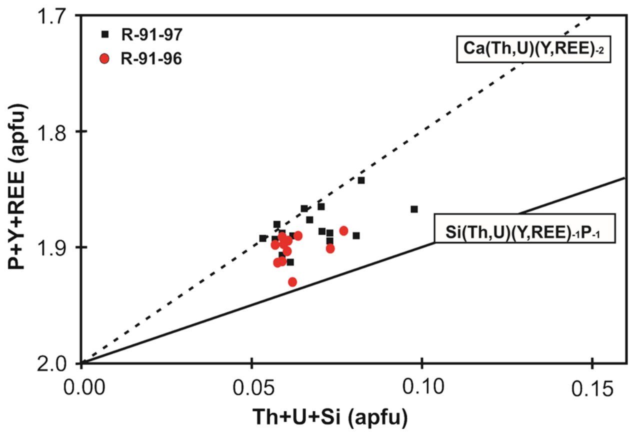

Figure 6. The bivariate plot shows the variation in the composition of monazite of two different granulite samples from Daltonganj (CGGC). Both rock types are enriched in the brabantite substitution vector as marked in the diagram.

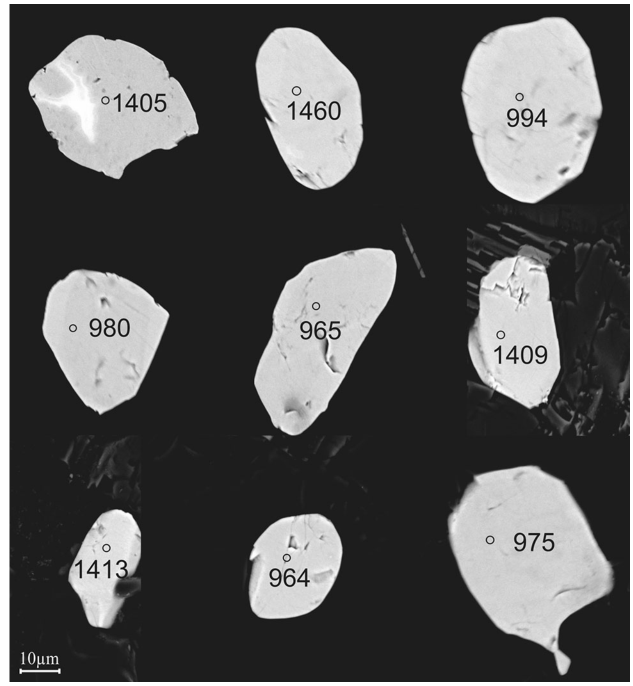

Figure 7. Represents the backscattered images (BSE-SEM) of different monazite grains from two rock samples.

Powell (1998), the P–T_{avg} was estimated for garnet–hypersthene–cordierite–biotite gneiss, the estimated average temperature and pressure (PT_{avg}) were 792°C and 7.35 kbar. The calculated pressure and temperature have corresponded to initial heating and compression until achieving a peak metamorphic condition, i.e., prograde metamorphism until the peak.

7. Discussion

7.1 *The timing of metamorphic events*

The CGGC has a multiplex metamorphic history, based on pre-existing geological information; the CGGC has been divided into four phases of metamorphic events (M_1–M_4). The M_1 metamorphic event is recorded at ∼1870 Ma from granulite enclaves emplaced in felsic gneiss; furthermore, the M_2 metamorphic event was dated between 1628 and 1270 Ma, where felsic magma intrusion occurred and further metamorphosed to form the migmatitic felsic gneiss. The M_3 phase is a high-grade metamorphic event that occurred during 1200–930 Ma, followed by the M_4 event (870–780 Ma) with the emplacement of the mafic dyke (Sanyal and Sengupta 2012 and references therein). The geochronological studies of various researchers from different localities of the CGGC, metamorphic phases (M_1–M_4), dating techniques and nature of rocks are compiled in table 1.

The P–T conditions during the M_1 metamorphic stage of the granulite facies rocks are difficult to derive due to their complex history of successive metamorphic events. Prograde granulite facies metamorphism was reported in the enclave suite (750–850°C/4–6 kbar), and this event was reported at >1500 Ma age by Maji *et al.* (2008). The P–T condition and the petrographic reaction texture relations are preserved within the rocks of the CGGC, which suggest the two prominent metamorphic events M_2 and M_3 that correspond to Mesoproterozoic and Grenvillian orogeny age (Sanyal and Sengupta 2012). These events represent the two different episodes of progressive metamorphism, which is separated by retrogressive metamorphic events (Maji *et al.* 2008), but the representative age is not distinguished. U–Pb zircon dating reveals that the age of intrusive A-type felsic magma (protolith of charnockite) is at 1447 + 11 Ma (Mukherjee *et al.* 2017), also during 1470–1450 Ma age, the emplacement of ferroan granitoids was reported in the north-eastern part of the CGGC (Mukherjee *et al.* 2018). A-type granitoid magmatism and fragmentation of the Columbia supercontinent are recorded during the Mesoproterozoic era (Hoffman 1989; Frost and Frost 2011). The monazite age (1424 ± 64 Ma) is revealed as the oldest age of the garnet–hypersthene–gedrite–cordierite

Table 7. *EPMA dating age of monazite crystals of granulites from the Daltonganj (Palamau) area.*

UO_2	ThO_2	PbO	Y_2O_3	Age (Ma)	Age err
Sample no. R-91-97					
0.280	3.526	0.261	0.351	1353	65
0.674	4.355	0.440	1.408	1482	49
0.348	5.690	0.423	2.042	1405	48
0.376	5.510	0.442	1.446	1481	51
0.564	4.747	0.394	1.406	1348	47
0.431	5.05	0.419	1.648	1460	51
Weighted mean age 1424 ± 64 Ma ($n = 6$, MSWD = 1.4, probability = 0.21).					
1.215	6.181	0.442	1.729	965	55
1.380	5.308	0.422	1.741	917	43
1.115	5.591	0.390	2.034	994	54
0.917	5.391	0.335	1.191	980	57
1.049	5.076	0.371	2.485	995	46
1.415	5.297	0.416	1.065	956	46
0.939	6.053	0.346	1.848	912	51
0.987	3.136	0.387	1.587	945	55
1.184	3.416	0.387	0.993	1029	61
0.904	5.406	0.385	0.565	1050	63
1.240	7.204	0.432	0.401	896	49
1.518	5.197	0.444	2.088	994	53
0.960	4.834	0.294	2.096	1049	48
1.009	3.372	0.276	1.890	985	60
Weighted mean age 972 ± 28 Ma ($n = 14$, MSWD = 0.55, probability = 0.47).					
Sample no. R-91-96					
0.258	3.921	0.316	0.914	1494	65
0.779	4.796	0.463	1.068	1409	44
0.279	3.516	0.258	0.402	1322	64
0.772	4.794	0.434	1.162	1331	43
0.591	6.072	0.459	0.599	1400	41
0.530	4.584	0.397	1.463	1413	50
Weighted mean age 1390 ± 56 Ma ($n = 6$, MSWD = 1.2, probability = 0.30).					
1.448	4.568	0.413	2.370	964	50
1.215	6.181	0.442	1.729	945	52
1.050	5.57	0.387	2.243	984	64
0.971	5.658	0.337	2.383	958	62
0.591	6.072	0.459	0.599	1019	59
1.034	5.098	0.365	2.124	983	61
1.121	5.500	0.398	2.219	926	58
1.144	5.228	0.383	2.021	933	54
0.883	5.802	0.266	1.170	975	51
1.415	5.297	0.416	1.065	938	52
0.591	6.072	0.459	0.599	990	60
1.144	5.577	0.437	2.329	965	51
1.034	5.098	0.365	2.124	938	58
Weighted mean age 962 ± 15 Ma ($n = 13$, MSWD = 0.88, probability = 0.57).					

gneiss; it is signified as the age of the gneissic protolith. The EPMA monazite ages 972 and 962 Ma (Grenville Orogeny) represent the high-grade granulite facies event, which is recorded in the Daltonganj. Petrographical features show that recrystallisation of the amphibole-rich magmatic rock to garnet-hypersthene-bearing gneiss by the following reaction during the M_3 event:

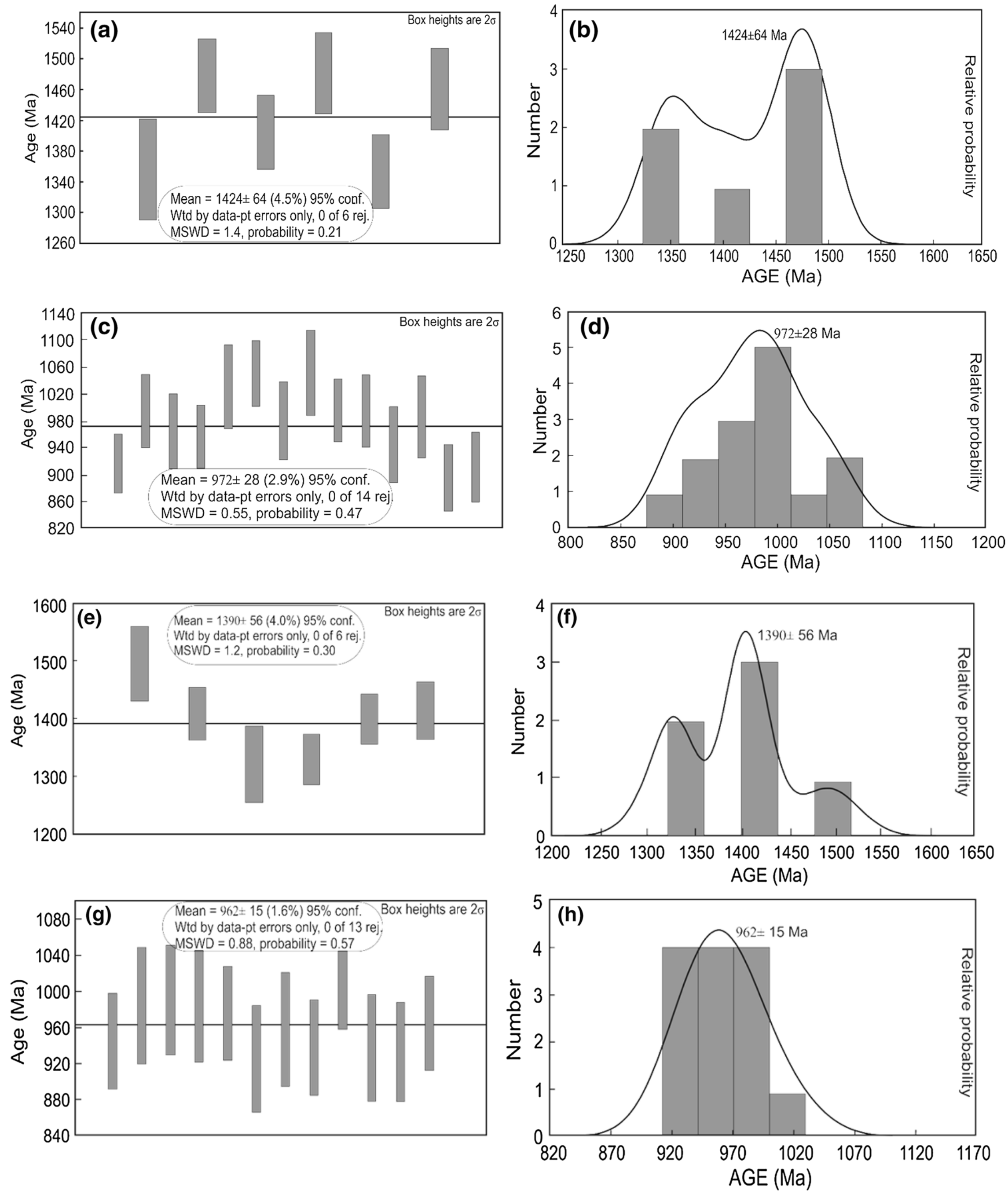

Figure 8. (**a**) and (**c**) Weighted-average ages (**b**) and (**d**) probability–density ages of two distinct age domains from the R-91-97 rock sample and (**e**) and (**g**) weighted-average ages and (**f**) and (**h**) probability–density ages of two distinct age domains from the R-91-96 rock sample with 2σ uncertainty, different numbers of point analysis and MSWD (mean square of weighted deviates) for monazite from the Daltonganj area of the CGGC, plotted with the ISOPLOT program (Ludwig 2011).

$$\text{Gedrite} + \text{quartz} = \text{Garnet} + \text{hypersthene} + \text{cordierite} + \text{albite} + H_2O.$$

The appearance of the hypersthene indicates that the low *P–T* condition has changed into a high *P–T* condition of granulite facies. The *P–T* condition and reaction texture are interpreted from the mineral assemblage, which shows that gedrite and quartz are consumed to produce the garnet + hypersthene + cordierite mineral phases through the prograde metamorphism. Similar *P–T* condition and Grenvillian orogenic age (975 ± 67 Ma) were obtained by Chatterjee and Ghose (2011) from Chianki village of the Daltonganj area present in the north-west of the CGGC.

Table 8. *Pressure and temperature estimates of the garnet–hypersthene–gedrite–cordierite–gneiss of the study area through conventional geothermobarometers and internally consistent data sets.*

Estimate of geothermometers (temperature in °C) at 7 kbar			Estimate of geobarometers (pressure in kbar) at 700°C			
Garnet–cordierite geothermometer			Garnet–cordierite–sillimanite–quartz geobarometer			
1.	Thompson (1976)	726			P-Mg	P-Fe
2.	Holdaway and Lee (1977)	699	1.	Thompson (1976)	5.91	6.33
3.	Wells (1979)	788	2.	Wells (1979)	7.34	6.38
4.	Perchuk *et al.* (1985)	706	3.	Nichols *et al.* (1992)	4.85	5.72
5.	Perchuk (1991)	703	4.	Perchuck *et al.* (1985)	6.57	
6.	Bhattacharya *et al.* (1988)	737	5.	Wells and Richardson (1980)		6.67
7.	Aranovich and Podlesskii (1989)	711	6.	Lal (1991)	4.80	
8.	Nichols *et al.* (1992)	656	7.	Aranovich and Podlesskii (1983, 1989)	6.87	
9.	Dwivedi *et al.* (1998)	746	8.	Average	6.06 ± 0.90	6.28 ± 0.35
10.	Average	719 ± 30				

Table 9. *Result of internally consistent geothermobarometry with THERMOCALC v-3.21 (Holland and Powell 1998).*

(Cordierite present reaction)			
Reactions used to calculate average temperature (T_{av}) (for $x(H_2O) = 1.0$)			
Independent set of reactions	T (°C)	Sd (T)	ln K
1) 2mgts + 3q = crd	604	1166	7.671
2) 2py + 3fs = 2alm + 3en	532	455	6.990
3) 2py + 3fcrd = 2alm + 3crd	641	215	12.639
4) 3fs + 3mgts = py + 2alm	632	938	11.143
	T_{av}	Sd	fit
Average temperature (°C)	602	47	1.01
Reactions used to calculate average (P_{av}) pressure (for $x(H_2O) = 1.0$)	P (kbar)	Sd (P)	ln K
5) 2py + 4alm + 9q = 6fs + 3crd	5.5	0.94	0.727
6) 2alm + en + 3q = 3fs + crd	5.9	1.11	−2.088
	P_{av}	Sd	fit
Average pressure (kbar)	5.56	0.93	0.61
Single end member diagnostic information of (P–T_{av})	601°C/5.6 kbar		
(Cordierite absent reaction)			
Reactions used to calculate average temperature (T_{av}) (for $x(H_2O) = 1.0$)			
Independent set of reactions	T (°C)	Sd (T)	ln K
1) fs + fctd = alm + H_2O	678	47	1.456
2) 2py + 3fs = 2alm + 3en	797	412	4.940
3) py + east = 2mgts + phl	782	427	−2.452
	T_{av}	Sd	fit
Average temperature (°C)	752	25	0.81
Reactions used to calculate average (P_{av}) pressure (for $x(H_2O) = 1.0$)	P (kbar)	Sd (P)	ln K
4) alm + 2en + east = 2py + ann	7.6	12.54	−4.160
5) en + 3fs + 2east = 2alm + 2phl	7.2	4.21	5.234
	P_{av}	Sd	fit
Average pressure (kbar)	7.40	0.90	0.5
Single-end member diagnostic information of (P–T_{av})	792°C/7.35 kbar		

Note: Mineral abbreviations are alm = almandine, ann = annite, crd = cordierite, en = enstatite, east = eastonite, fcrd = ferro-cordierite, fs = ferrosillite, mgts = Mg-Tschermak pyroxene, q= quartz, phl = phlogopite, py = pyrope and H_2O= water fluid.

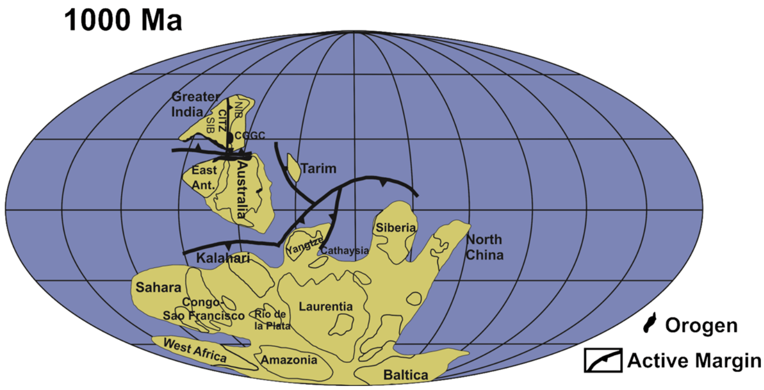

Figure 9. Cartographic picture showing the Rodinia assembly and position of India at ∼1000 Ma (modified after Li *et al.* 2008).

7.2 *Implications for the supercontinental history*

The age of formation, amalgamation and reconstruction of central and eastern Indian terrain generates essential information regarding the palaeogeographic condition of supercontinents. Rogers and Santosh (2002) proposed that the Columbia supercontinent amalgamation initiated ∼1900–1800 Ma and achieved their highest packing strength at 1600–1500 Ma and started to rift after 1500 Ma. During this rifting period a lot of magmatic processes were obtained, viz., crystallisation of anorthosite around 1550 Ma (Chatterjee *et al.* 2008), khondalite emplaced in the quartzo-feldspathic matrix around 1510 Ma (Sanyal *et al.* 2007), as well as charnockite gneiss emplacement during 1457 ± 63 Ma (Ray Barman *et al.* 1994). The development of Rodinia started from the Grenvillian orogenic age ∼1100–900 Ma, and drifting was started after 750 Ma. The number of configurations and models of the Rodinia supercontinent have been proposed by different scientists, including Dalziel (1991), Hoffman (1991), Rogers (1996), Meert (2001), Wingate *et al.* (2002) and Li *et al.* (2008). The age of fragmentation from 1200 to 800 Ma was interpreted within the southern Indian granulite blocks (Yoshida *et al.* 2003) at some locations. Ghose (1983) and Banerji (1991) mentioned orogenic phases in the CGGC, named as the Chhotanagpur orogeny (1600–1500 Ma) and the Satpura orogeny (900–850 Ma). However, the CGGC of eastern India shows a shred of evidence of the Grenvillian-orogeny age at 1100–900 Ma which is strongly preserved, and it postulates that the Grenvillian-orogeny suture was very near the CGGC of India. In the previously proposed models, Greater India was emplaced along the western side of East Antarctica and the SW part of Australia to produce a substantial accretionary mass of western Rodinia (Dalziel 1991; Hoffman 1991; Moores 1991). They suggested that India was assembled with the Rodinia supercontinent through the continent–continent collision between 1000 and 900 Ma along the Eastern Ghats mobile belt (EGMB) and CGGC of the Indian subcontinent which corresponds to East Antarctica's Rayner Province. Li *et al.* (2008) explained the palaeolatitudinal position between Greater India and the Australian land mass at ∼770–750 Ma age due to the drifting of the Indian plate away from the Australia–East Antarctica continental plate by ca. 755 Ma. The transpressional movement of the Indian and Australian continental plates may explain the 1100–1000 Ma metamorphic events investigated from the Pinjarra orogen (Bruguier *et al.* 1999; Fitzsimons 2003). The (∼1424 Ma) older age reveals the age of emplacement of felsic magmatism similar to the rocks of the other area of the CGGC that has been mentioned in table 1. This rock was assumed to be the protolith of granulitic gneiss, which was formed by the high-grade metamorphism under granulite facies conditions ('Grenville-age' orogenesis, 1000–900 Ma) during M_3 in Daltonganj, presumably during the assembly of Rodinia. The 1000 Ma high-grade metamorphism gives evidence of tectono-metamorphic episodes in the CGGC, CITZ and EGMB of India (figure 9).

8. Conclusion

The CGGC represents a complex metamorphic history, where Mesoproterozoic metamorphism was overlain by high-grade metamorphism of Grenvillian-orogeny (1100–900 Ma). The CGGC terrain mainly contains high-grade amphibolite facies to granulite facies rocks, which lies between two medium- to low-grade mobile belts. The north-western part of the CGGC depicts that the protolith of granulitic gneiss had been emplaced around 1424 Ma age and subsequently transformed by a high-grade metamorphic event at 972 Ma. High-grade metamorphism at 972–962 Ma from the Daltonganj area of the north-western CGGC suggests connecting link between the Satpura mobile belts of CITZ in Grenvillian-orogeny. The *P–T* condition calculated in the present study perhaps corresponds to initial heating and compression until achieving a peak metamorphic condition. The prograde metamorphic condition in the Daltonganj area of the CGGC at the M_3 metamorphic event has reported 7.35 kbar/792°C in the Grenvillian age. Thus, Grenvillian metamorphism was well documented in the CGGC, where Greater India was part of the Rodinia supercontinent.

Acknowledgements

We are thankful to the Director, Indian Institute of Technology (BHU) for providing the infrastructure and funds to complete this work. R Kumar is also grateful to the UGC–JRF scheme for providing financial support for the present work. The authors express their gratitude to Prof N V Chalapathi Rao and Dr Dinesh Pandit from Mantle Petrology Laboratory, Department of Geology, Centre of Advanced Study, Institute of Science, BHU, for providing the EPMA and SEM analyses facility. We are also thankful to the Associate Editor, Prof P Sengupta and the anonymous reviewers for their constructive comments and useful suggestions to improve the quality of the manuscript.

References

Acharyya S K 2003 The nature of Mesoproterozoic central Indian tectonic zone with exhumed and reworked older granulites; *Gondwana Res.* **6**(**2**) 197–214.

Aranovich L Ya and Podlesskii K K 1983 The cordierite–garnet–sillimanite equilibrium: Experiments and application; In: *Kinetics and equilibrium in mineral reactions* (ed.) Saxena S K, Springer, New York, Berlin, Heidelberg, Tokyo, pp. 173–198.

Aranovich L Ya and Podlesskii K K 1989 Geothermobarometry of high-grade metapelites: Simultaneously operating reactions; In: *Evolution of metamorphic belts* (eds) Cliff R A, Yardley B D and Daly J S, Blackwell Scientific Publications, Oxford; *Geol. Soc. Spec. Publ.* **43** 45–61.

Bhattacharya A, Mazumdar A C and Sen S K 1988 Fe–Mg mixing in cordierite: Constraints from natural data and implications for cordierite–garnet geothermometry in granulites; *Am. Mineral.* **73** 338–344.

Banerji A K 1991 Presidential address. Geology of the Chhotanagpur region; *Indian J. Geol.* **63** 275–282.

Bhowmik S K, Bernhardt H J and Dasgupta S 2010 Grenvillian age high-pressure upper amphibolite Granulite metamorphism in the Aravalli–Delhi Mobile Belt, Northwestern India: New evidence from monazite chemical age and its implication; *Precamb. Res.* **178** 168–184.

Bhowmik S K, Wilde S A, Bhandari A and Sarbadhikari A B 2014 Zoned Monazite and zircon as monitors for the thermal history of Granulite Terranes: An example from the central Indian tectonic zone; *J. Petrol.* **55** 585–621.

Braun I, Montel J M and Nicollet C 1998 Electron microprobe dating of monazites from high-grade gneisses and pegmatites of the Kerala Khondalite Belt, southern India; *Chem. Geol.* **146** 65–85.

Bruguier O, Bosch D, Pidgeon R T, Byrne D I and Harris L B 1999 U–Pb chronology of the Northampton complex, Western Australia: Evidence for Grenvillian sedimentation, metamorphism and deformation and geodynamic implications; *Contrib. Mineral. Petrol.* **136** 258–272.

Cocherie A, Legendre O, Peucat J J and Kouamelan A 1997 *In-situ* Th-U-Pb dating using an electron microprobe: A powerful tool for complex polygenic monazites; *Terra Abst.* **9** 441.

Chatterjee N, Crowley J L and Ghose N C 2008 Geochronology of the 1.55 Ga Bengal anorthosite and Grenvillian metamorphism in the Chhotanagpur gneissic complex, eastern India; *Precamb. Res.* **161** 303–316.

Chatterjee N, Banerjee M, Bhattacharya A and Maji A K 2010 Monazite chronology, metamorphism-anatexis and tectonic relevance of the mid-Neoproterozoic Eastern Indian tectonic zone; *Precamb. Res.* **179** 99–120.

Chatterjee N and Ghose N C 2011 Extensive early Neoproterozoic high-grade metamorphism in North Chhotanagpur gneissic complex of the central Indian tectonic zone; *Gondwana Res.* **20** 362–379.

Dalziel I W D 1991 Pacific margins of Laurentia and East Antarctica–Australia as a conjugate rift pair: Evidence and implications for an Eocambrian supercontinent; *Geology* **19**(**6**) 598–601.

Dasgupta S and Sengupta P 2003 Indo-Antarctic correlation: A perspective from the Eastern Ghats Granulite Belt, India; In: *Proterozoic East Gondwana: Supercontinent assembly and breakup* (eds) Yoshida M, Windley B E, Dasgupta S, *Geol. Soc. London, Spec. Publ.* **206** 131–143.

Dwivedi S B, Mohan A and Lal R K 1998 Recalibration of Fe–Mg exchange reaction between garnet and cordierite as a thermometer; *Eur. J. Mineral.* **10** 281–289.

Dwivedi S B, Kumar R R and Srivastava M 2019 Multistage gedrite in gedrite–hypersthene bearing high-grade granulites from Daltonganj, Chhotanagpur granite gneissic complex, Jharkhand, as evident from TEM and textural relations; *J. Earth Syst. Sci.* **128**(**41**) 1–14.

Fitzsimons I C W 2003 Proterozoic basement provinces of southern and southwestern Australia, and their correlation with Antarctica; *Geol. Soc. London, Spec. Publ.* **206** 93–130.

Frost C D and Frost B R 2011 On ferroan (A-type) granitoids: Their compositional variability and modes of origin; *J. Petrol.* **52** 39–53.

Ghose N C 1983 Geology, tectonics and evolution of the Chhotanagpur granite–gneiss complex, Eastern India; In: *Structure and tectonics of Precambrian Rocks of India* (ed.) Sinha-Roy S, *Recent Res. Geol. v.10*, Hindustan Publ. Corp., Delhi, pp. 211–247.

Ghose N C 1992 Chhotanagpur gneiss–granulite complex, Eastern India: Present status and future prospect; *Indian J. Geol.* **84** 100–121.

Hoffman P F 1989 Speculations on Laurentia's first giga year (2.0 to 1.0 Ga); *Geology* **17** 135–138.

Hoffman P F 1991 Did the breakout of Laurentia turn Gondwanaland inside out? *Science* **252** 1409–1412.

Holdaway M J and Lee S M 1977 Fe–Mg cordierite stability in high natural pelitic rocks based on experimental, theoretical and natural observations; *Contrib. Mineral. Petrol.* **63** 175–198.

Holland T J B and Powell R 1998 An internally-consistent thermodynamic dataset for phases of petrological interest; *J. Met. Geol.* **16** 309–344.

Karmakar S, Bose S, Sarbadhikari A B and Das K 2011 Evolution of granulite enclaves and associated gneisses from Purulia, Chhotanagpur granite gneiss complex, India: Evidence for 990–940 Ma tectonothermal event(s) at the eastern India cratonic fringe zone; *J. Asian Earth Sci.* **41** 69–88.

Lal R K 1991 Ti content of mica as a geothermobarometry; In: *Third Indo-Soviet Symposium on Experimental Mineralogy and Petrology*, New Delhi, pp. 13–15.

Li Z X, Bogdanova S V, Collins A S, Davidson A, De Waele B, Ernst R E, Fitzsimons I C W, Fuck R A, Gladkochub D P, Jacobs J, Karlstrom K E, Lu S, Natapov L M, Pease V, Pisarevsky S A, Thrane K and Vernikovsky V 2008 Assembly, configuration, and break-up history of Rodinia: A synthesis; *Precamb. Res.* **160** 179–210.

Ludwig K R 2011 *Isoplot 3.70 (version-4): A geochronological toolkit for microsoft excel*; Berkeley Chronology Center, Berkeley, California, Special Publication 4.

Maji A K, Goon S, Bhattacharya A, Mishra B, Mahato S and Bernhardt H J 2008 Proterozoic polyphase metamorphism in the Chhotanagpur gneissic complex (India) and implication for trans-continental Gondwanaland correlation; *Precamb. Res.* **162** 385–402.

Mallik A K, Gupta S N and Ray Barman T 1991 Dating of early Precambrian granite–greenstone complex of the Eastern Indian Precambrian shield with special reference to the Chhotanagpur granite gneiss complex; *Rec. Geol. Survey India* **124** 20–21.

Meert J G 2001 Growing Gondwana and rethinking Rodinia: A paleomagnetic perspective; *Gondwana Res.* **4(3)** 279–288.

Mezger K and Cosca M A 1999 The thermal history of the Eastern Ghats Belt (India) as revealed by U–Pb and $^{40}Ar/^{39}Ar$ dating of metamorphic and magmatic minerals: Implications for the SWEAT correlation; *Precamb. Res.* **94** 251–271.

Montel J M, Veschambre M and Nicollet C 1994 Datation de la monazite a la microsonde électronique; *Comptes Rendus – academie des sciences parisserie 2 sciences de la terre et desplanetes fascicule a.* **318** 1489–1495.

Montel J, Foret S, Veschambre M, Nicollet C and Provost A 1996 Electron microprobe dating of monazite; *Chem. Geol.* **131** 37–53.

Moores E M 1991 Southwest US–east antarctic (SWEAT) connection: A hypothesis; *Geology* **19** 425–428.

Mukherjee S, Dey A, Sanyal S, Ibanez-Mejia M, Dutta U and Sengupta P 2017 Petrology and U–Pb geochronology of zircon in a suite of charnockitic gneisses from parts of the Chhotanagpur granite gneiss complex (CGGC): Evidence for the reworking of a Mesoproterozoic basement during the formation of the Rodinia supercontinent; In: *Crustal evolution of India and Antarctica: The supercontinent connection, Geological Society of London, special publications* (eds) Pant N C and Dasgupta S, *Geol. Soc. London, Spec. Publ.,* https://doi.org/10.1144/sp457.6.

Mukherjee S, Dey A, Ibanez-Mejia M, Sanyal S and Sengupta P 2018 Geochemistry, U–Pb geochronology and Lu–Hf isotope systematics of a suite of ferroan (A-type) granitoids from the CGGC: Evidence for Mesoproterozoic crustal extension in the east Indian shield; *Precamb. Res.* **305** 40–63.

Nichols G T, Berry R F and Green D H 1992 Internally consistent gahnitic spinel cordierite-garnet equilibria in the FMASHZn system: Geothermobarometry and application; *Contrib. Mineral. Petrol.* **111** 362–377.

Pabst A and Hutton C O 1951 Huttonite, a new monoclinic thorium silicate; *Am. Mineral.* **36** 60–69.

Pandey B K, Upadhyaya L D and Sinha K K 1986a Geochronology of Jajawal–Binda–Nagnaha granitoids in relation to uranium mineralization; *Indian J. Earth Sci.* **13** 163–168.

Pandey B K, Gupta J N and Lall Y 1986b Whole rock and mineral Rb–Sr isochron ages for the granites from Bihar mica belt of Hazaribagh, Bihar, India; *Indian J. Earth Sci.* **13** 157–162.

Pandey M, Pandit D, Arora D, Chalapathi Rao N V and Pant N C 2019 Analytical protocol for U–Th–Pb chemical dating of monazite using CAMECA SX Five EPMA installed at the Mantle Petrology Laboratory, Department of Geology, Banaras Hindu University, Varanasi, India; *J. Geol. Soc. India* **93** 46–50.

Parrish R R 1990 U–Pb dating of monazite and its application to geological problems; *Can. J. Earth Sci.* **27** 760–763.

Perchuk L L 1991 Derivation of a thermodynamically consistent set of geothermometers and geobarometers for metamorphic and magmatic rocks; In: *Progress in metamorphic and magmatic petrology (A memorial volume in honor of DS Korzhinsky)* (ed.) Perchuk L L, Cambridge University Press, Cambridge, pp. 93–112.

Perchuk L L, Aranovich L Ya, Podlesskii K K and Lavrenteva I V 1985 Precambrian granulites of the Alden Shield. Eastern Siberia USSR; *J. Met. Geol.* **3** 265–310.

Prabhakar N 2013 Resolving poly-metamorphic Paleoarchean ages by chemical dating of monazites using multi-spectrometer U, Th and Pb analyses and sub-counting methodology; *Chem. Geol.* **347** 255–270.

Ray Barman T and Bishui P K 1994 Dating of Chhotanagpur gneissic complex of eastern Indian Precambrian shield; *Rec. Geol. Surv. India* **127(2)** 25–27.

Ray Barman T, Bishui P K and Mukhopadhyay Ray J N 1994 Rb–Sr geochronology of the high-grade rocks from Purulia, West Bengal and Jamua–Dumka sector, Bihar; *Indian Mineral.* **48** 45–60.

Roy A and Devarajan M K 2000 A reappraisal of the stratigraphy and tectonics of the Palaeoproterozoic Mahakoshal supracrustal belt, Central India. *Proceedings of the International Seminar on Precambrian Crust in Eastern and Central India*, UNESCOIUGS-IGCP 368; *Geol. Surv. India, Spec. Publ.* **57** 79–97.

Rode K P 1948 On the charnockite rocks of Palamau, Bihar, India; *Schweizerische Mineralogische and Petrographische Mitteilungen.* **28** 288–302.

Rogers J J W 1996 A history of continents in the past three billion years; *J. Geol.* **104** 91–107.

Rogers J J W and Santosh M 2002 Configuration of Columbia, a Mesoproterozoic supercontinent; *Gondwana Res.* **5** 5–22.

Rosa-Costa L T D, Lafon J M, Cocherie A and Delor C 2008 Electron microprobe U–Th–Pb monazite dating of the Transamazonian metamorphic overprint on Archean rocks from the Amapá Block, southeastern Guiana Shield, Northern Brazil; *J. South Am. Earth Sci.* **26** 445–462.

Rose D 1980 Brabantite, $CaTh[PO_4]_2$, a new mineral of the monazite group; *Neues Jahrb. Mineral., Monatsh.* **6** 247–257.

Saha A K 1994 Crustal evolution of Singhbhum–North Orissa, Eastern India; *J. Geol. Soc. India Memoir* **27** 341.

Saikia A, Gogoi B, Kaulina T, Lialina L, Bayanova T and Ahmad M 2017 Geochemical and U–Pb zircon age characterization of granites of the Bathani Volcano Sedimentary sequence, Chhotanagpur granite gneiss complex, eastern India: Vestiges of the Nuna supercontinent in the central Indian tectonic zone; In: *Crustal evolution of India and Antarctica: The supercontinent connection* (eds) Pant N C and Dasgupta S, *Geol. Soc. London, Spec. Publ.* **457**.

Sanyal S, Sengupta P and Goswami R 2007 Evidence of Mesoproterozoic ultra-high temperature Metamorphism from parts of CGGC, Jharkhand, India; In: *Abstract volume of the International Conference on Precambrian sedimentation and tectonics and second GPSS meeting,* Indian Institute of Technology, Bombay, pp. 62–63.

Sanyal S and Sengupta P 2012 Metamorphic evolution of the Chhotanagpur granite gneiss complex of the East Indian Shield: Current status; In: *Palaeoproterozoic of India* (eds) Mazumder R and Saha D, *Geol. Soc. London, Spec. Publ.* **365** 117–145.

Sarkar S N 1980 Precambrian stratigraphy and geochronology of Peninsular India: A review; *Indian J. Earth Sci.* **7** 12–26.

Schaltegger U, Fanning C M, Gunther D, Maurin J C, Schulmann K and Gebauer D 1999 Growth, annealing and recrystallization of zircon and preservation of monazite in high-grade metamorphism: Conventional and *in-situ* U–Pb isotope, cathodoluminescence and microchemical evidence; *Contrib. Mineral. Petrol.* **134** 186–201.

Shaw R K, Arima M, Kagami H, Fanning C M, Shiraishi K and Motoyoshi Y 1997 Proterozoic events in the Eastern Ghats Granulite Belt, India: Evidence from Rb–Sr, Sm–Nd systematics, and shrimp dating; *J. Geol.* **105** 645–656.

Singh R N, Thorpe R and Kristic D 2001 Galena Pb isotope date of base metal occurrences in the Hesatu–Belbathan belt, eastern Precambrian shield, Bihar; *J. Geol. Soc. India* **57** 535–538.

Singh Y and Krishna V 2009 Rb–Sr Geochronology and petrogenesis of granitoids from the Chhotanagpur granite gneiss complex of Raikera–Kunkuri region, central India; *J. Geol. Soc. India.* **74** 200–208.

Spear F S and Pyle J M 2010 Theoretical modeling of monazite growth in a low-Ca metapelite; *Chem. Geol.* **273** 111–119.

Suzuki K and Adachi M 1991 Precambrian provenance and Silurian metamorphism of the Tsubonasawa paragneiss in the South Kitakami terrane, Northeast Japan, revealed by the Chemical Th–U total lead isochron ages of monazite, zircon and xenotime; *Geochem. J.* **25** 357–376.

Suzuki K and Adachi M 1994 Middle Precambrian detrital monazite and zircon from the Hida gneiss on Oki–Dogo island, Japan: Their origin and implications for the correlation of basement gneiss of Southwest Japan and Korea; *Tectonophys.* **235** 277–292.

Thompson A B 1976 Mineral reactions in pelitic rocks: I. Prediction of P–T–X (Fe–Mg) phase relations. II. Calculations of some P–T–X (Fe–Mg) phase relations; *Am. J. Sci.* **276** 401–454.

Wells P R A 1979 Chemical and thermal evolution of Archean sialic crust, southern Greenland; *J. Pet.* **20** 187–226.

Wells P R A and Richardson S W 1980 Thermal evolution of metamorphic rocks in the central Highlands of Scotland; In: *The Caledonides of the British Isles–reviewed* (eds) Harris A L, Holland C H and Leake B E, *Geol. Soc. London, Spec. Publ.* **8** 339–344.

Whitney D L and Evans B W 2010 Abbreviations for names of rock-forming minerals; *Am. Mineral.* **95** 185–187.

Williams M L, Jercinovic M J and Terry M 1999 High resolution 'age' mapping, chemical analysis, and chemical dating of monazite using the electron microprobe: A new tool of tectonic analysis; *Geology* **27** 1023–1026.

Wingate M T D, Pisarevsky S A and Evans D A D 2002 Rodinia connections between Australia and Laurentia: No SWEAT, no AUSWUS? *Terra Nova* **14** 121–128.

Yadav B S, Wanjari N, Ahmad T and Chaturvedi R 2016 Geochemistry and petrogenesis of Proterozoic granitic rocks from northern margin of the Chhotanagpur gneissic complex (CGC); *J. Earth Syst. Sci.* **125** 1041–1060.

Yoshida M, Funaki M and Vitanage P W 1992 Proterozoic to Mesozoic East Gondwana: The Juxtaposition of India, Sri Lanka, and Antarctica; *Tectonics* **11** 381–391.

Yoshida M, Jacobs J, Santosh M and Rajesh H M 2003 Pan-African events in the Circum-East Antarctic Orogen of East Gondwana: A critical overview; In: *Proterozoic East Gondwana: Supercontinent assembly and breakup* (eds) Yoshida M, Windley B F and Dasgupta S, *Geol. Soc. London, Spec. Publ.* **206** 57–75.

Corresponding editor: N V Chalapathi Rao